Science Bulletin 64 (2019) 1750–1756

Contents lists available at ScienceDirect

Science Bulletin

journal homepage: www.elsevier.com/locate/scib

Article

Local engineering of topological phase in monolayer MoS_2

Zhichang Wang [a,1], Xiaoqiang Liu [a,1], Jianqi Zhu [b,c,1], Sifan You [a], Ke Bian [a], Guangyu Zhang [b,d,e,*], Ji Feng [a,d,f,*], Ying Jiang [a,d,f,*]

[a] International Center for Quantum Materials, School of Physics, Peking University, Beijing 100871, China
[b] Beijing National Laboratory for Condensed Matter Physics and, Institute of Physics, Chinese Academy of Sciences, Beijing 100190, China
[c] School of Physics and Electronic Engineering, Sichuan Normal University, Chengdu 610101, China
[d] Collaborative Innovation Center of Quantum Matter, Beijing 100190, China
[e] School of Physical Sciences, University of Chinese Academy of Sciences, Beijing 100190, China
[f] CAS Center for Excellence in Topological Quantum Computation, University of Chinese Academy of Sciences, Beijing 100190, China

ARTICLE INFO

Article history:
Received 17 August 2019
Received in revised form 23 September 2019
Accepted 3 October 2019
Available online 10 October 2019

Keywords:
Phase engineering
Quantum spin Hall insulator
Transition metal dichalcogenides
Edge states
Phase boundary

ABSTRACT

Monolayer transition metal dichalcogenides (TMDCs) with the 1T′ structure are a new class of large-gap two-dimensional (2D) topological insulators, hosting topologically protected conduction channels on the edges. However, the 1T′ phase is metastable compared to the 2H phase for most of 2D TMDCs, among which the 1T′ phase is least favored in monolayer MoS_2. Here we report a clean and controllable technique to locally induce nanometer-sized 1T′ phase in monolayer 2H-MoS_2 via a weak Argon-plasma treatment, resulting in topological phase boundaries of high density. We found that the stabilization of 1T′ phase arises from the concerted effects of S vacancies and the tensile strain. Scanning tunneling spectroscopy (STS) clearly reveals a spin-orbit band gap (~60 meV) and topologically protected in-gap states residing at the 1T′-2H phase boundary, which are corroborated by density-functional theory (DFT) calculations. The strategy developed in this work can be generalized to a large variety of TMDCs materials, with potentials to realize scalable electronics and spintronics with low dissipation.

1. Introduction

Two-dimensional (2D) topological insulators (TIs) are also known as quantum spin Hall (QSH) insulators, in which the topologically protected conduction channels at the edges support the dissipationless charge/spin transport [1–7]. So far, only a few QSH insulators have been reported in experiments, such as HgTe [4,7], InAs quantum wells [2], and Bi bilayers [8]. However, the band gaps of these 2D TIs are very small, greatly limiting their application at realistic temperatures. Recently, 2D transition metal dichalcogenides (TMDCs) with 1T′ structure were predicted to be a new family of large-gap QSH insulators [6]. Structure distortion in 1T′ phase leads to an intrinsic band inversion and the spin-orbit coupling (SOC) opens a gap in the bulk. Characteristics of 2D time-reversal invariant TI such as helical edge states, quantum conductance of the edge and suppression of the edge conduction by magnetic field have been demonstrated in monolayer 1T′-WTe_2 [9,10], which displays a positive QSH gap [11]. In addition, angle-resolved photoemission spectroscopy (ARPES) and scanning tunneling spectroscopy (STS) have shown signatures of topological band inversion and band-gap opening of monolayer 1T′-WTe_2 [12–14]. Very recently, 1T′-WSe_2 was also found to be a new QSH insulator with topological edge states by combined ARPES and STS measurements [15,16].

Unfortunately, the 1T′ phase is only metastable while the 2H phase is thermodynamically stable for most of the 2D TMDCs, among which monolayer MoS_2 is least favored energetically [6,17]. The formation energy of 1T′-MoS_2 is about 0.55 eV higher than that of the 2H phase, and thus it is very challenging to grow and stabilize MoS_2 in the 1T′ phase. It has been shown that the 2H → 1T′ phase transition of monolayer TMDCs can be induced by alkali ion intercalation [18–20], laser irradiation [21,22], or electrostatic gating [23]. However, a scalable, controllable and nondestructive method for engineering the topological phase of monolayer MoS_2 is still lacking and the helical edges states are yet to be explored [24,25]. In this work, we use a clean and weak Argon-plasma treatment approach to induce 1T′ phase locally in monolayer 2H-MoS_2 grown on highly oriented pyrolytic graphite (HOPG). We found that the stabilization of 1T′ phase arises from the concerted effects of S vacancies and the tensile strain. Scanning

* Corresponding authors.
E-mail addresses: gyzhang@iphy.ac.cn (G. Zhang), jfeng11@pku.edu.cn (J. Feng), yjiang@pku.edu.cn (Y. Jiang).
[1] These authors contributed equally to this work.

https://doi.org/10.1016/j.scib.2019.10.004
2095-9273/

tunneling microscopy (STM) topography verifies the distorted octahedral structure of the 1T′ phase and STS reveals that the 1T′ phase has a bulk bandgap about 60 meV and in-gap states residing at the 2H-1T′ phase boundary. Density functional theory (DFT) calculations further confirm the nontrivial topological nature of the boundary states.

2. Experimental

2.1. CVD growth of monolayer MoS_2

A three zone furnace is used for CVD growth of MoS_2. Sulfur (S) (Alfa Aesar 99.9%) and molybdenum trioxide (MoO_3) (Alfa Aesar 99.999%) were used as precursors and loaded in zone Ⅰ and Ⅱ, respectively. The distance between the two sources was 20 cm. The temperatures of MoO_3 and S were 530 and 115 °C, respectively. HOPG was used as growth substrates, put in the third zone. MoS_2 growth was conducted at 0.93 Torr under an Ar flow rate of 130 sccm for 10 min.

2.2. Argon-plasma treatment

Argon-plasma treatment was performed in a home-made, remote plasma system [26]. An inductively coupled plasma was generated by dispersing a 20-W RF power at the entrance of a 4-inch quartz-tube furnace using a RF (13.56 MHz) coil. The as-grown MoS_2 samples were placed at the center of the furnace, separated from the RF coil region by a distance of ≈15 in. The pressure in the tube furnace was fixed at ~0.69 Torr for phase transition by flowing Argon at 100 sccm and vacuum pumping. The process was carried out for different time at room temperature.

2.3. STM and STS measurements

STM/S experiments were performed in an cryogenic ultrahigh-vacuum STM system (Createc, Germany) with base pressure $<7 \times 10^{-9}$ Pa. Electrochemically etched W-tips were cleaned by alternative annealing and sputtering before the experiments, and further by controlled field-emission and voltage-pulse procedures during the scanning. Before STM investigations, the samples were cleaned *in situ* by heating it up to 300 °C for an extended time (typically overnight). Bias voltage refers to the sample voltage with respect to the tip. All of the STM topographic images were obtained in constant-current mode at 77 and 5 K. The STS (d*I*/d*V* spectra) were acquired at 5 K with the feedback loop off, using lock-in detection of the tunnelling current by adding a 5-mV_{rms} modulation at 481 Hz to the sample bias.

3. Results and discussion

3.1. Phase engineering via weak Argon-plasma treatment

Fig. 1 shows the morphology evolution of the monolayer 2H-MoS_2 undergoing the Argon-plasma treatment. Monolayer MoS_2 has three different phases with distinct electronic characteristics [19]. Depending on the arrangement of S atoms and Mo atoms,

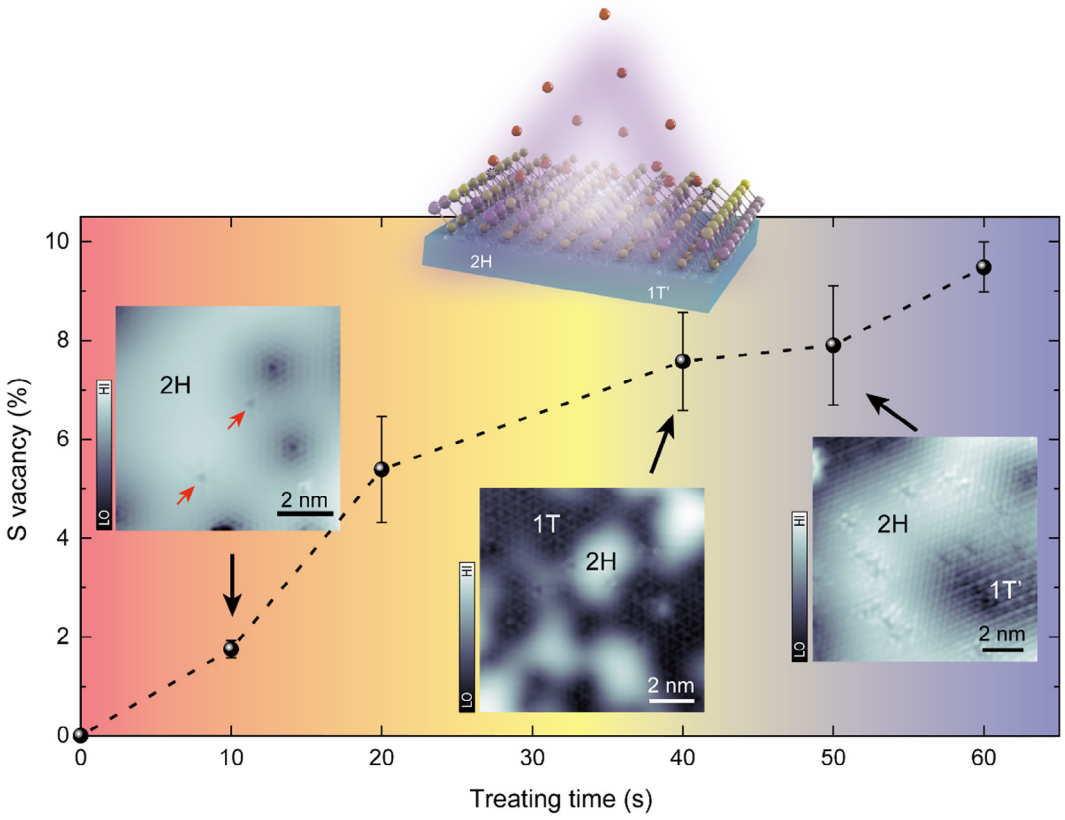

Fig. 1. Phase engineering of monolayer MoS_2 via weak Argon-plasma treatment. Main panel: the density of sulfur vacancies as a function of Argon-plasma treating time. The sulfur vacancy percentage is determined via dividing the number of S vacancies in STM image by the calculated total amount of S atoms on the surface in the STM image. The error bar is obtained from statistics of different regions on the surface. Insets: schematic illustration of Argon-plasma treatment of monolayer MoS_2 (upper) and typical STM images of plasma-treated MoS_2 with different treating time (lower). The single sulfur vacancies are denoted by red arrows in leftmost STM image (t = 10 s). The regions corresponding to three different phases (2H, 1T, and 1T′) are marked in the STM images. Set points of STM images: 0.8 V, 10 pA (t = 10 s); 1.5 V, 5 pA (t = 40 s); 0.6 V, 15 pA (t = 50 s).

single-layer MoS_2 shows different symmetries: 2H phase (trigonal prismatic D_{3h}), 1T phase (octahedral O_h) and 1T′ phase (distorted octahedral $P2_1/m$). The three phases can inter-convert from one to another. S atoms of one plane sliding laterally from the hexagonal vertex to the center [27] results in the transition from 2H to 1T (Fig. 2a and b). Distortion of the Mo atoms in 1T phase along ***b*** direction leads to a period-doubling 2×1 distorted structure with zigzag Mo-chains in the ***a*** direction [6,28], i.e. 1T′ structure (Fig. 2c). Before the plasma treatment, STM and STS reveal a perfect hexagonal structure and a large band gap about 2.5 eV (Fig. 2a and d), as expected for the 2H phase. Note that STM images can only reflect the arrangement of the S atoms in the top layer of monolayer MoS_2 [29].

At the initial stage of the plasma treatment, we found that small scattered depressions arise, accompanied with a small amount of S vacancies (see the red arrows in Fig. 1, $t = 10$ s). The bombardment of argon ions (in the plasma) with low kinetic energy first kick away surface-layer S atoms and result in surface-layer S vacancies. The sub-layer Mo atoms and S atoms are protected by the surface-layer S atoms. Increasing the treating time leads to the increased concentration of S vacancies. Meanwhile, the size of the depression regions also increases, forming mosaic structures (Fig. 1, $t = 40$ s). The depression regions show the same atomic structure as the 2H phase (Fig. 2b), but with a metallic character (Fig. 2e). Detailed STM measurements clearly display the lateral sliding of S atoms in the dark regions with respect to the bright regions (2H phase), confirming that the dark regions should correspond to the 1T phase (Fig. S1a online). Further increasing the treating time introduces even more S vacancies, and some of the dark regions exhibit chain-like structures with a percentage of ~30% (Fig. 1, $t = 50$ s). High-resolution STM topography denotes a period-doubling 2×1 distortion and alternative up/down of the S atoms rows (Fig. 2c), which is the structural characteristic of 1T′ phase. Indeed, STS measurements show a distinct band gap about 60 meV (Fig. 2f), which

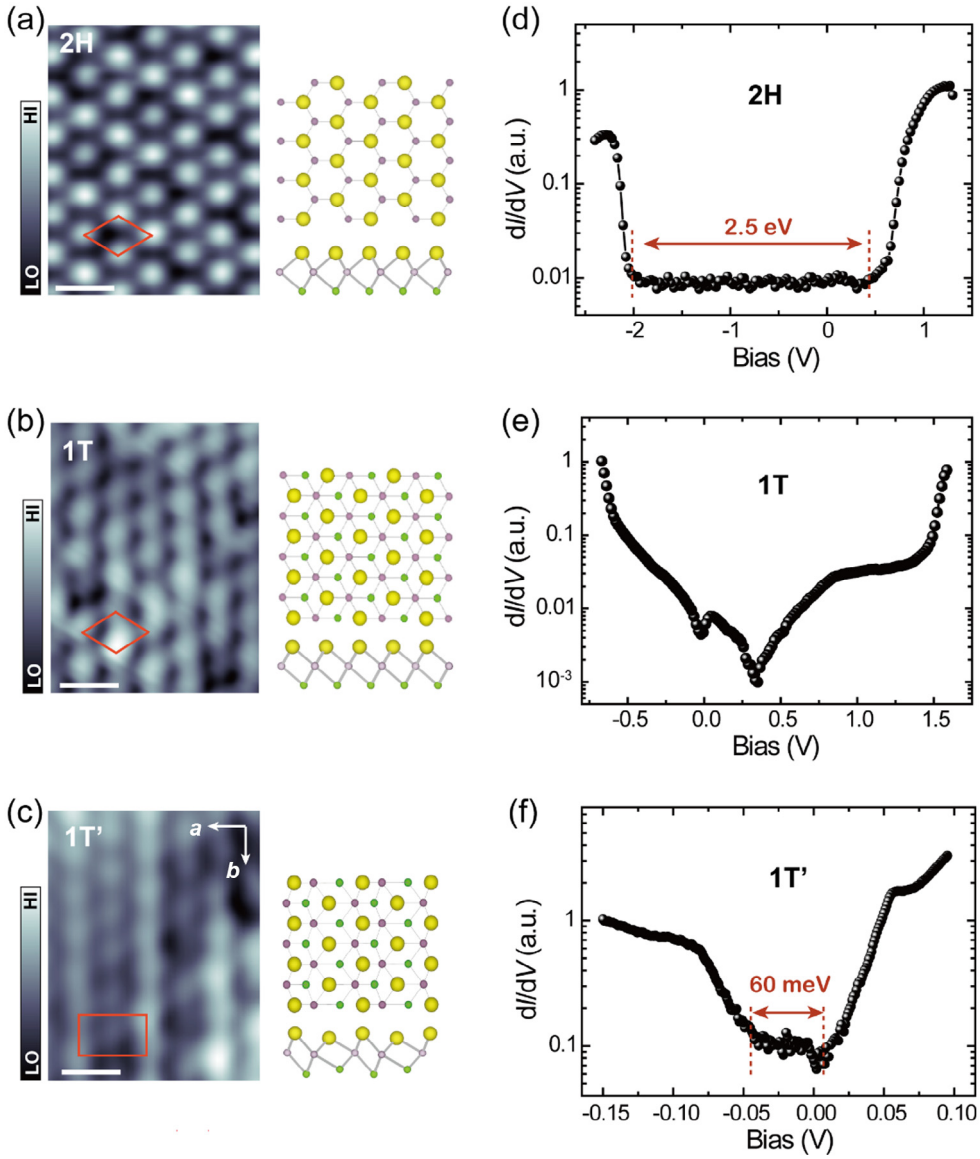

Fig. 2. Atomic and electronic structure of monolayer MoS_2 in different phases. (a)–(c) STM topographic images of monolayer MoS_2 in 2H, 1T and 1T′ phases, respectively. Structural models in top view and side-view models are displayed on the rightside of STM images. Mo: purple; top S: yellow; bottom S: green. The unit cells of different phases are depicted by red lines. For the 1T′ phase, the Mo atoms are distorted in ***a*** direction ([1 0 0]), resulting in alternative up and down of surface S atom rows in ***b*** direction ([1 2 0]). (d)–(f) d*I*/d*V* spectra of 2H, 1T and 1T′ phases, respectively. The band gaps are denoted in (d) and (f). Set points of STM images: (a): 0.7 V, 500 pA; (b): 0.7 V, 5 pA; (c): 0.6 V, 20 pA. Set points of d*I*/d*V* spectra: (d): 1.5 V, 50 pA; (e): 1.5 V, 50 pA; (f): 0.1 V, 10 pA. Scale bar in (a)–(c): 0.5 nm.

is consistent with the theoretical prediction of band-gap opening due to the SOC effects in 1T′ phase [6]. DFT calculations usually underestimate charge transfer band gap but give a reasonable result for spin–orbit band gap. The residual conductance in the gap is due to that electrons can tunnel from the tip directly into the conducting HOPG substrate. In fact, Fig. 2d and f have different set points. In order to get large enough signal-to-noise ratio of gapped dI/dV at low bias for 1T′ phase, tip needs to get closer to the surface, resulting in more electrons tunneling into HOPG substrate and a more prominent residual conductivity originating from HOPG substrate (Fig. 2f) compared to that in Fig. 2d. Increasing the bombardment time to several minutes or increasing the kinetic energy of argon ions could produce deeper-layer vacancies, and even damage the monolayer MoS_2 film. Therefore, we can achieve nondestructive phase transition by controlling the bombardment time and the kinetic energy of argon ions.

It has been demonstrated that the stabilization of 1T′ phase is related to the existence of chalcogen vacancy, which reduces the formation energy of 1T′ phase with respect to 2H phase [22,28,30]. When the concentration of chalcogen vacancy reaches a certain level, the energy of 1T′ phase can be even lower than 2H phase [22]. The transition from 2H to 1T′ is clearly correlated with the increasing density of S vacancies (Fig. 1), which do not dramatically change the electronic structure of MoS_2 and introduce deep in-gap states [31] (Fig. S2 online). This is possibly due to that the vacancies are filled by some other alien atoms such as oxygen [32]. In addition, we also found that the atomic lattice of 2H phases near the 1T/1T′ phases are slightly strained, leading to the narrowing of the band gap [33] (Fig. S3 online). Therefore, it is likely that the S vacancies and tensile strain both contribute to the stabilization of 1T′ phase [17,22]. The bombardment of argon ions has two effects: first, it induces S vacancies to make 1T′ phase thermodynamically more stable; second, it provides kinetic energy to overcome the barrier for phase transition from 2H phase to 1T′ phase. Such a phase-engineering method can be easily extended to other family members of TMDCs.

3.2. Calculated band structures of 2H-1T′ heterostructure

The next, we investigate the electronic structure of the 2H-1T′ heterostructure. There are four non-degenerate domain boundary structures in light of the sliding direction of the S atoms with respect to the domain boundary (Fig. S4 online). The side-sliding modes (stretched "4,5" and compressed "2,3") have lower energies (~0.445 eV) than the vertical-sliding modes ("1,6"). Therefore, we only consider the side-sliding modes, which can be identified in the atomic-resolution STM image (Fig. S1b online). Such a kind of 2H-1T′ heterostructure model is shown in Fig. 3a, where S atoms in the middle region of the upper plane of monolayer MoS_2 slide in ***b*** direction and zigzag Mo-chains are along ***a*** direction. The resulting 1T′ phase is connected to two 2H phases, forming a stretched boundary on the left and a compressed boundary on the right.

The band structures of the heterostructure obtained by DFT calculations are shown in Fig. S5 (online). Strongly localized edge states connect the conduction band and valence band of 1T′ phase. Fig. 3b and c show blow-up views of band structure near the Fermi surface, with the red dots indicating the weight of the bands on either boundary of the 2H-1T′-2H junction. Clearly in both cases, the edge bands connect the bulk conduction band and valence band near $q = 0$, and are doubly degenerate at $q = 0$ and $q = \pi/b$. The degeneracy at $q = 0$ of edge states at the stretched boundary is removed due to small magnetic moment on Mo localized at this boundary (Fig. 3b). More important, for either edge, the bands localized on it cross the Fermi level an odd number of times (Fig. 3b and c); this indicates that the boundary separating the 1T′ and 2H is boundary between topologically distinct regions. Knowing that the 2H phase MoS_2 is topologically trivial, this is a

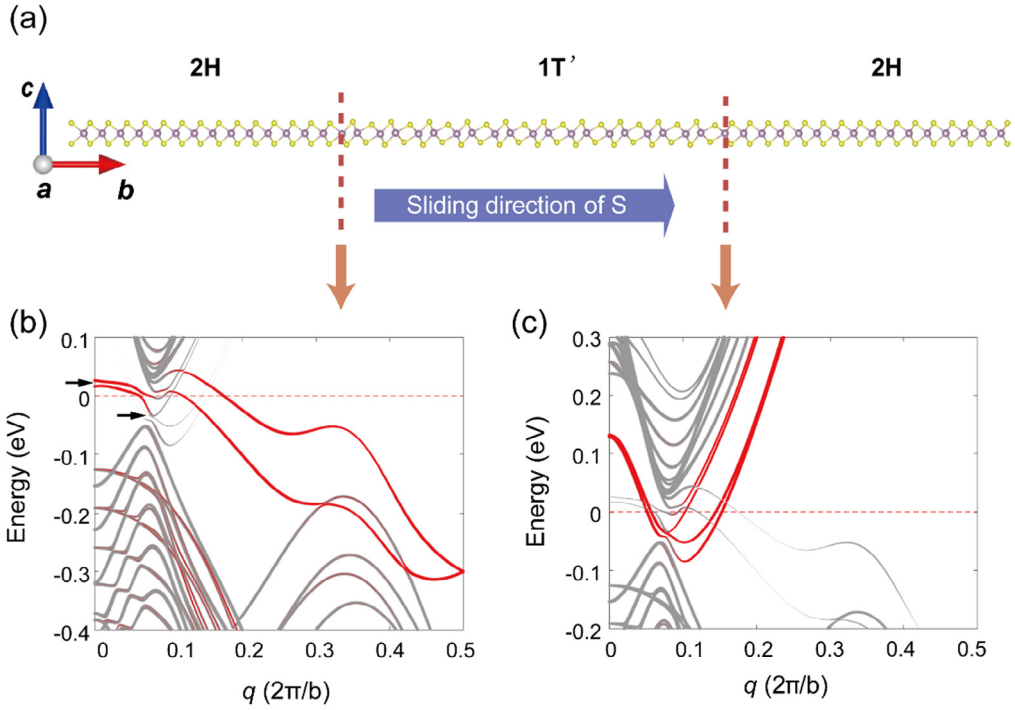

Fig. 3. Calculated band structure of 2H-1T′-2H heterostructure. (a) Atomic model of the 2H-1T′-2H heterostructure. S atoms in the upper plane of monolayer 1T′-MoS_2 slide in ***b*** direction and the zigzag Mo-chains are along ***a*** direction. (b), (c) Zoom-in band dispersion near the Fermi surface to highlight the edge states localized at the left and right phase boundaries, respectively. The red dots represent the edge states, while the gray dots represent the bulk states. The edge states go through Fermi level odd times, indicating its nontrivial topological nature. The black arrows in (b) denote the flat band at $q = 0$ and the turning point at $q \approx 0.33$ of the topological edge states.

clear indication of the topological nature of the 1T′ phase, even when the region of 1T′ is as narrow as several nanometers.

3.3. STS measurements of edge states residing at 2H-1T′ boundary

In order to verify the existence of the edge states in the 2H-1T′ heterostructure, we performed STS measurements across the phase boundary for two different heterophase structures, where the S-sliding and Mo-distorting directions with respect to the phase boundary are different (Figs. 4 and S7 (online)). The phase boundary shown in Fig. 4a belongs to the stretched side-sliding domain boundary (see Fig. S1b (online) for details). The bulk 1T′ phase has a band gap about 60 meV, which is consistent with the DFT calculation (the lower panel of Fig. 4b). Interestingly, the STS spectrum taken at the phase boundary shows intensive states in the gap, i.e. nonvanishing density of base states and two prominent peaks (highlighted by the blue arrows in the upper panel of Fig. 4b), with one near the conduction band edge of 1T′ phase (~+0.02 eV) and the other close to valence band edge (~−0.04 eV).

The calculated local density of states (LDOS) (Fig. 4b, red curves) qualitatively agree with the experimental dI/dV (Fig. 4b, black curves). The band structures at the boundary (blue line in Fig. S5 online) and within 1T′ bulk (green line in Fig. S5 online) are very different, resulting in different characters in LDOS. On the phase boundary, there are non-negligible LDOS around the Fermi level and vanishing LDOS at the conduction and valence bands. Within the 1T′ bulk, on the contrary, a prominent gap is visible and the LDOS of the conduction and valence bands are high. The two peaks in the calculated LDOS at the phase boundary are originated from the flat band at q = 0 and the turning point at q ≈0.33 of the topological edge states (marked by black arrows in Fig. 3b) and the non-zero base intensity originates from the topological band with a slope within the band gap. The existence of in-gap states is required by the different topological nature of 2H and 1T′ phase. The quantitative discrepancy between the experimental dI/dV and the calculated LDOS may arise from the defects, strain and contribution from the conducting substrate. Those features also exist for the other type of phase boundary (see Fig. S7 online), suggesting the robustness of the topologically protected edge states. By performing STS mapping, we further determined that the penetration depth of the boundary states into the 1T′ phase is about 2 nm (Fig. 4c, S6 and S8 (online)).

4. Conclusions and implication

It is noted that the edge states reside at the phase boundary within the bulk of monolayer MoS_2 rather than exposed edges, which suffer from structural disorders and contaminations [2,4,9,10]. The weak-plasma treatment developed in this work can be easily generalized to a large variety of 2D TMDCs materials, where the 1T′ phase is considerably less stable than the 2H phase. Combined with shadow mask or focused ion/e-beam/laser-beam pattern techniques [22,27], it is possible to pattern well-defined strips of 1T′ phase within 2H phase and built topological circuits consisting of highly dense one-dimensional conduction channels which has recently been achieved by laser beam irradiation in thin MoS_2 film [21]. However laser beam irradiation is destructive to monolayer films [21,22]. Furthermore, we can use top gate to control on and off of these channels by applying a vertical electric field to induce topological phase transition [6,34]. Such a strategy is fully compatible with the state-of-the-arts lithography techniques, which may facilitate the realization of highly integrated and scalable electronics and spintronics with low dissipation. We note that only nanometer-sized 1T′ islands have been achieved in the current work, which is not quite suitable for electronic device. Future efforts should be geared toward more controlled

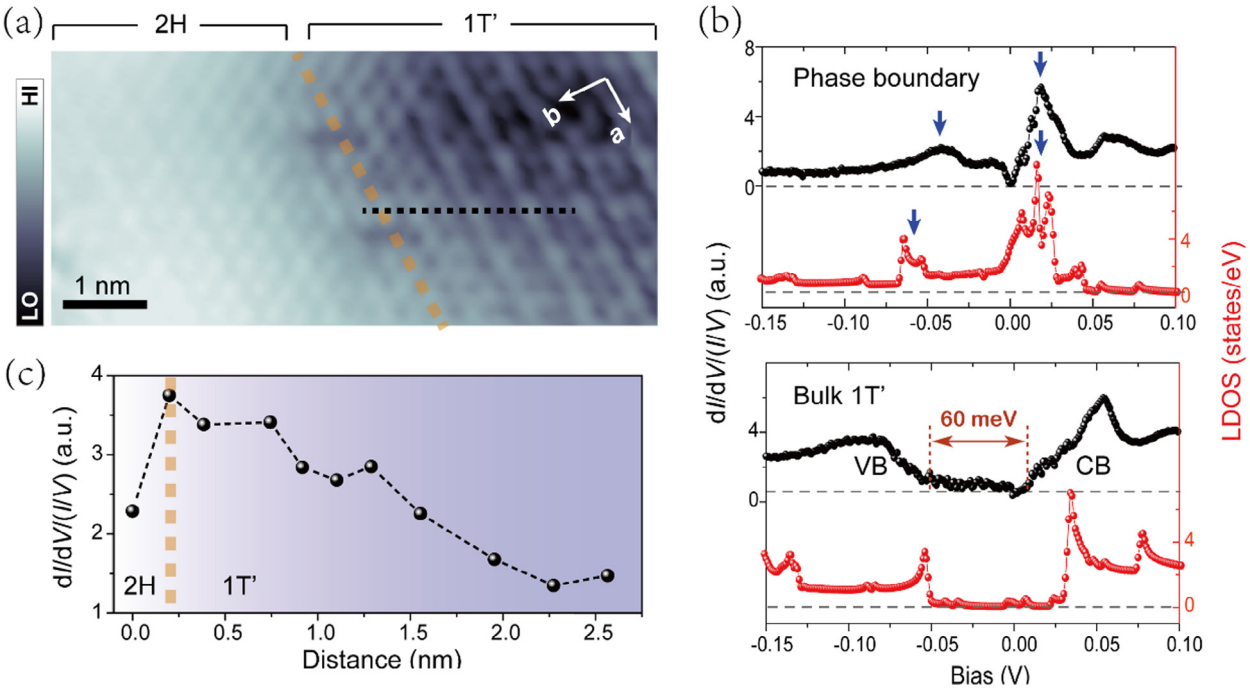

Fig. 4. STS measurements of the edge states at the 2H-1T′ phase boundary. (a) STM image of the 2H-1T′ heterophase structure, corresponding to the stretched side-sliding domain boundary. The orange dotted line denotes the phase boundary. (b) dI/dV spectra (black) and calculated LDOS (red) in the bulk 1T′ (lower panel) and on the phase boundary (upper panel). In order to highlight in-gap states, the dI/dV spectra are normalized by I/V. The two in-gap states are denoted by blue arrows. The conduction band and valence band of 1T′ phase are denoted as CB and VB, respectively. (c) dI/dV mapping of the edge state (at V = −50 mV) as a function of the distance across the phase boundary (see the black dotted line in (a), which indicates that the edge states penetrate into the 1T′ phase for about 2 nm. Set point of the STM image (a): 0.6 V, 20 pA. Set point of the dI/dV spectra (b): −500 pm referenced to the set point of (1 V, 5 pA).

engineering of 1T′ phase by decoupling the MoS_2 from the substrate and exploring the current synthetic route with other TMDs, which have a smaller energy difference between 2H and 1T′ phase.

Conflict of interest

The authors declare that they have no conflict of interest.

Acknowledgments

This work was financially supported by the National Natural Science Foundation of China (11888101, 11634001, 11834017 and 61888102), the National Key R&D Program (2016YFA0300901 and 2017YFA0205003), the Strategic Priority Research Program of Chinese Academy of Sciences (XDB28000000 and XDB30000000), and Beijing Municipal Science & Technology Commission. Y.J. acknowledges support from National Science Fund for Distinguished Young Scholars (21725302) and Cheung Kong Young Scholar Program.

Author contributions

Ying Jiang designed and supervised the study. Zhichang Wang, Sifan You and Ke Bian performed the STM experiments. Jianqi Zhu and Guangyu Zhang prepared the samples. Xiaoqiang Liu and Ji Feng performed the DFT calculations. Zhichang Wang, Xiaoqiang Liu, Jianqi Zhu, Ji Feng, Guangyu Zhang and Ying Jiang analyzed the data. Zhichang Wang and Ying Jiang wrote the manuscript with the input from all the other authors. The manuscript reflects the contributions of all authors.

Appendix A. Supplementary materials

Supplementary materials to this article can be found online at https://doi.org/10.1016/j.scib.2019.10.004.

References

[1] Hasan MZ, Kane CL. Colloquium: topological insulators. Rev Mod Phys 2010;82:3045–67.
[2] Knez I, Du RR, Sullivan G. Evidence for helical edge modes in inverted InAs/GaSb quantum wells. Phys Rev Lett 2011;107:136603.
[3] Bernevig BA, Zhang SC. Quantum spin Hall effect. Phys Rev Lett 2006;96:106802.
[4] Bernevig BA, Hughes TL, Zhang SC. Quantum spin Hall effect and topological phase transition in HgTe quantum wells. Science 2006;314:1757–61.
[5] Kane CL, Mele EJ. Quantum spin Hall effect in graphene. Phys Rev Lett 2005;95:226801.
[6] Qian XF, Liu JW, Fu L, et al. Quantum spin Hall effect in two-dimensional transition metal dichalcogenides. Science 2014;346:1344–7.
[7] Konig M, Wiedmann S, Brune C, et al. Quantum spin Hall insulator state in HgTe quantum wells. Science 2007;318:766–70.
[8] Hirahara T, Bihlmayer G, Sakamoto Y, et al. Interfacing 2D and 3D topological insulators: Bi(111) bilayer on Bi_2Te_3. Phys Rev Lett 2011;107:166801.
[9] Fei ZY, Palomaki T, Wu SF, et al. Edge conduction in monolayer WTe_2. Nat Phys 2017;13:677–82.
[10] Wu SF, Fatemi V, Gibson QD, et al. Observation of the quantum spin hall effect up to 100 kelvin in a monolayer crystal. Science 2018;359:76–9.
[11] Zheng FP, Cai CY, Ge SF, et al. On the quantum spin Hall gap of monolayer 1T′-WTe_2. Adv Mater 2016;28:4845–51.
[12] Tang SJ, Zhang CF, Wong D, et al. Quantum spin Hall state in monolayer 1T′-WTe_2. Nat Phys 2017;13:683–7.
[13] Jia ZY, Song YH, Li XB, et al. Direct visualization of a two-dimensional topological insulator in the single-layer 1T′-WTe_2. Phys Rev B 2017;96:041108.
[14] Peng L, Yuan Y, Li G, et al. Observation of topological states residing at step edges of WTe_2. Nat Commun 2017;8:659.
[15] Chen P, Pai WW, Chan YH, et al. Large quantum-spin-Hall gap in single-layer 1T′ WSe_2. Nat Commun 2003;2018:9.
[16] Ugeda MM, Pulkin A, Tang S, et al. Observation of topologically protected states at crystalline phase boundaries in single-layer WSe_2. Nat Commun 2018;9:3401.
[17] Duerloo KAN, Li Y, Reed EJ. Structural phase transitions in two-dimensional Mo- and W-dichalcogenide monolayers. Nat Commun 2014;5:4214.
[18] Eda G, Fujita T, Yamaguchi H, et al. Coherent atomic and electronic heterostructures of single-layer MoS_2. ACS Nano 2012;6:7311–7.
[19] Kan M, Wang JY, Li XW, et al. Structures and phase transition of a MoS_2 monolayer. J Phys Chem C 2014;118:1515–22.
[20] Liu LN, Wu JX, Wu LY, et al. Phase-selective synthesis of 1T′ MoS_2 monolayers and heterophase bilayers. Nat Mater 2018;17:1108–14.
[21] Mine H, Kobayashi A, Nakamura T, et al. Laser-beam patterned topological insulating states on thin semiconducting MoS_2. arXiv:180704914, 2018.
[22] Cho S, Kim S, Kim JH, et al. Phase patterning for ohmic homojunction contact in $MoTe_2$. Science 2015;349:625–8.
[23] Wang Y, Xiao J, Zhu HY, et al. Structural phase transition in monolayer $MoTe_2$ driven by electrostatic doping. Nature 2017;550:487–91.
[24] Xu H, Han D, Bao Y, et al. Observation of gap opening in 1T′ phase MoS_2 nanocrystals. Nano Lett 2018;18:5085–90.
[25] Yin XM, Wang QX, Cao L, et al. Tunable inverted gap in monolayer quasi-metallic MoS_2 induced by strong charge-lattice coupling. Nat Commun 2017;8:486.
[26] Zhu JQ, Wang ZC, Yu H, et al. Argon plasma induced phase transition in monolayer MoS_2. J Am Chem Soc 2017;139:10216–9.
[27] Lin YC, Dumcencon DO, Huang YS, et al. Atomic mechanism of the semiconducting-to-metallic phase transition in single-layered MoS_2. Nat Nanotechnol 2014;9:391–6.
[28] Keum DH, Cho S, Kim JH, et al. Bandgap opening in few-layered monoclinic $MoTe_2$. Nat Phys 2015;11:482–6.
[29] Huang YL, Chen YF, Zhang WJ, et al. Bandgap tunability at single-layer molybdenum disulphide grain boundaries. Nat Commun 2015;6:6298.
[30] Park JC, Yun SJ, Kim H, et al. Phase-engineered synthesis of centimeter-scale 1T′- and 2H-molybdenum ditelluride thin films. ACS Nano 2015;9:6548–54.
[31] Li H, Tsai C, Koh AL, et al. Activating and optimizing MoS_2 basal planes for hydrogen evolution through the formation of strained sulphur vacancies. Nat Mater 2016;15:48–53.
[32] Barja S, Refaely-Abramson S, Schuler B, et al. Identifying substitutional oxygen as a prolific point defect in monolayer transition metal dichalcogenides. Nat Commun 2019;10:3382.
[33] Shin BG, Han GH, Yun SJ, et al. Indirect bandgap puddles in monolayer MoS_2 by substrate-induced local strain. Adv Mater 2016;28:9378–84.
[34] Tong QJ, Yu HY, Zhu QZ, et al. Topological mosaics in moire superlattices of van der waals heterobilayers. Nat Phys 2017;13:356–62.

Zhichang Wang received his Ph.D. degree from Peking University in 2018, under the supervision of Ying Jiang. He is now a postdoctoral in Xiamen University and visiting scholar in Institute of Applied Physics of TU Wien, Austria. His research interests include surface physics and surface chemistry in ferroelectrics and perovskite oxides and advancing the application of scanning probe microscopy/spectroscopy into exotic surface.

Guangyu Zhang received a Ph.D. degree from the Institute of Physics, Chinese Academy of Sciences, in 2004. From 2004–2008, he has been in Stanford University as a postdoc researcher. In 2008, he joined the Institute of Physics, Chinese Academy of Sciences as a faculty. Now he is the director of Nanoscale Physics and Devices Laboratory in Institute of Physics, Chinese Academy of Sciences and deputy director of Songshan Lake Materials Laboratory in Guangdong. His current research interests are low dimensional (especially 2D) materials with focusing on their novel electronic and mechanical properties and related device applications.

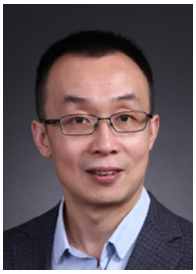

Ji Feng obtained his Ph.D. degree in 2007 at Cornell University. After that, he went on to postdoctoral positions at Harvard University and then at University of Pennsylvania. In 2011, he joined the faculty of International Center for Quantum Materials and School of Physics at Peking University, where he is now a full Professor. His research covers electronic structure theory and methods for extended solids, including materials modeling and developing computational toolkits for novel physical properties.

Ying Jiang received his Ph.D. degree from Institute of Physics, Chinese Academy of Sciences (CAS) in 2008. After working as a Postdoctoral Associate in University of California, Irvine (2008–2010), he joined International Center for Quantum Materials, Peking University as a tenure-track assistant professor, and was promoted to full professor in 2018. Ying Jiang is an expert in advanced scanning probe microscopy/spectroscopy and focused on the atomic-scale properties and ultrafast dynamics in single molecules and low-dimensional materials.